Journal of Inorganic Biochemistry 189 (2018) 17–29

Contents lists available at ScienceDirect

Journal of Inorganic Biochemistry

journal homepage: www.elsevier.com/locate/jinorgbio

BODIPY-based Ru(II) and Ir(III) organometallic complexes of avobenzone, a sunscreen material: Potent anticancer agents

Gajendra Gupta[a,d,*], Shirisha Cherukommu[b], Gunda Srinivas[b], Seon Woong Lee[a], Sung Hwan Mun[c], Jaehoon Jung[c], Narayana Nagesh[b,*], Chang Yeon Lee[a,d,**]

[a] Department of Energy and Chemical Engineering, Incheon National University, 119 Academy-ro, Yeonsu-gu, Incheon 22012, Republic of Korea
[b] CSIR-Centre for Cellular and Molecular Biology, Hyderabad 500007, India
[c] Department of Chemistry, University of Ulsan, Ulsan 44610, Republic of Korea
[d] Innovation Center for Chemical Engineering, Incheon National University, 119 Academy-ro, Yeonsu-gu, Incheon 22012, Republic of Korea

ARTICLE INFO

Keywords:
Avobenzone
Bodipy
Ruthenium complexes
Iridium complexes
Anticancer properties

ABSTRACT

The use of organic compounds with known medicinal properties in the synthesis of metal-based complexes is an important alternative to improve the biological activity of metal-based drugs. The reaction of $[M(arene)Cl_2]_2$ (M = Ru, arene = *p-cymene* and M = Ir, arene = pentamethylcyclopentadienyl, *cp**) with avobenzone (1-(4-*tert*-butylphenyl)-3-(4-methoxyphenyl)propane-1,3-dione, AVBH) and KOH in methanol leads to the formation of the neutral complexes [Ru(*p-cymene*)(AVB)Cl] **1** and [Ir(*cp**)(AVB)Cl] **2** (*cp** = pentamethylcyclopentadienyl). Subsequent reaction of **1** and **2** with pyridyl derivative-BODIPY ligands, BDP and BDPCC (BODIPY = boron dipyrromethene, BDP = 4-dipyridine boron dipyrromethene, BDPCC = 4-ethynylpyridine boron dipyrromethene) in methanol gives a series of four new dicationic supramolecules: $[Ru_2(p\text{-}cymene)_2(AVB)_2BDP][2CF_3SO_3]$ **3**, $[Ir_2(cp^*)_2(AVB)_2BDP][2CF_3SO_3]$ **4**, $[Ru_2(p\text{-}cymene)_2(AVB)_2BDPCC][2CF_3SO_3]$ **5** and $[Ir_2(cp^*)_2(AVB)_2BDPCC][2CF_3SO_3]$ **6**. The synthesized complexes are fully characterized using multiple analytical techniques, including elemental analysis, ^1H NMR, ^{13}C NMR, ^{19}F NMR (NMR = Nuclear Magnetic Resonance), Infrared Radiation (IR), Electrospray Ionization-Mass Spectrometry (ESI-MS), Ultraviolet-visible (UV–Vis) and fluorescence spectroscopy. The structures of these complexes are further rationalized using density functional theory (DFT) calculations. The antiproliferative activity of the neutral and dinuclear cationic complexes is evaluated in vitro in different human cancer cell lines. These complexes are found to be active against different cancer cell lines with half maximal inhibitory concentration (IC_{50}) values between 1 and 5 μM. Complexes **5** and **6** displayed the lowest IC_{50} values in all the cell lines studied. The activity of **5** and **6** is comparable to that of the well-known chemotherapy drug doxorubicin. Detailed biophysical studies indicate that complexes **5** and **6** exhibit very good Deoxyribonucleic acid (DNA) binding properties, causing the unwinding of the double helix, which is a probable reason for their high cytotoxicity.

1. Introduction

According to the World Health Organization, cancer is the second largest cause of death in developed nations, and the estimated annual cancer death toll will exceed 13 million by 2030 [1]. Metal-based drugs are very important compounds in treating cancer, and platinum complexes in particular are widely used in cancer treatment [2]. Despite their widespread use, platinum-based drugs have severe side effects that are often as painful as the disease itself [3]. In order to avoid these severe side effects, and to overcome drug resistance during the chemotherapy procedure, complexes based on metals other than platinum have emerged as a special research focus. Ruthenium complexes have shown especially promising results due to the interesting properties of the ruthenium metal center [4]. Ruthenium complexes have been shown to be less toxic than platinum based complexes, and appear to work by a different mode of action [5]. The biological activity of arene-ruthenium based metal complexes is being studied by several groups [6]. Two Ru-based anticancer drugs, imidazolium trans-[tetrachlorido(dimethylsulfoxide)(1H-imidazole)ruthenate(III)] (NAMI-A) and indazolium trans-[tetrachloridobis(1H-indazole)ruthenate(III)]

* Corresponding authors.
** Correspondence to: C.Y. Lee, Innovation Center for Chemical Engineering, Incheon National University, 119 Academy-ro, Yeonsu-gu, Incheon 22012, Republic of Korea.
E-mail addresses: gjngupt@gmail.com (G. Gupta), nagesh@ccmb.res.in (N. Nagesh), cylee@inu.ac.kr (C.Y. Lee).

https://doi.org/10.1016/j.jinorgbio.2018.08.009
Received 17 March 2018; Received in revised form 8 August 2018; Accepted 9 August 2018
Available online 16 August 2018
0162-0134/

(KP1019), which were developed by Sava and Keppler, respectively, are already in clinical trials, which further indicates the promising future of metal-based complexes [7]. Since the discovery of these two important ruthenium metal complexes, many groups have been actively working on the biological applications of transition metal complexes [8]. The structure and properties of cyclopentadienyl iridium complexes are often considered to be similar to those of their arene ruthenium analogues. Although, the biological side of iridium complexes are not as well-studied as those of ruthenium analogues, several half-sandwich iridium complexes have shown greater potency than cisplatin against various cancer cell lines [9].

An important strategy to improve the biological activity is by employing organic ligands with known biological properties to develop new metal complexes [10]. In these direction, herein, we combine a highly fluorescent BODIPY (boron dipyrromethene) ligand with avobenzone (1-(4-*tert*-butylphenyl)-3-(4-methoxyphenyl)propane-1,3-dione, AVBH), an oil soluble compound used as sunscreen agent and in cosmetic products, to develop new dicationic ruthenium and iridium supramolecules. Recent studies have shown that AVBH has promising antiproliferative activity against different human cancer cell lines [11]. Additionally, the dye BODIPY has been vividly studied for more than three decades due to its excellent photo-physical and chemical properties. The BODIPY-based ligands were chosen on the basis of their important applications in cancer therapy due to their absorption and emission properties, which helps in biological labeling experiments for the detection of tagged entities in and around biological cells [12]. To combine the advantages of AVBH and BODIPY ligands, we designed new dicationic ruthenium (II) and iridium (III) based supramolecules by incorporating dipyridyl BODIPY ligands in ruthenium and iridium AVBH complexes. The biological activities of these supramolecules were investigated and the BDPCC (4-ethynylpyridine boron dipyrromethene) based ruthenium and iridium molecules were found to have more potent anticancer properties than the BDP (4-dipyridine boron dipyrromethene) containing supramolecules.

2. Results and discussion

2.1. Synthesis and characterization

The neutral mononuclear organometallic complexes **1** and **2** were synthesized by the reaction of $[Ru(p\text{-cymene})Cl_2]_2$ and $[Ir(cp^*)Cl_2]_2$ dimers with avobenzone in the presence of KOH in methanol (Scheme 1). Further details of the syntheses of these complexes are provided in experimental section. Both complexes were neutral and were obtained as a yellow solid in high yield. The complexes were highly soluble in common organic solvents, and were stable both in air and in solution. The ^{1}H NMR spectroscopy was initially used to confirm the formation of these complexes. The ^{1}H NMR spectra in $CDCl_3$ showed all the required protons which supported the formation of the expected structures and the values are given in the experimental section. Electrospray ionization (ESI) mass spectroscopy was further studied which displayed peaks corresponding to the loss of the chloride ion attached to the metal. Peaks were observed at 545.14 and 637.13 amu for complex **1** and **2** respectively (Fig. S1(a), (b)).

The reaction of mononuclear complex **1** with the BODIPY ligands BDP and BDPCC in methanol under nitrogen at room temperature afforded dinuclear complexes **3** and **5**, respectively (Scheme 2). Complexes **3** and **5** were obtained as their triflate salts, and were non-hygroscopic and stable in air and solution. The complxes were soluble in common polar solvents such as dichloromethane, chloroform, methanol, ethanol, acetone and acetonitrile but were insoluble in hexane, diethylether and petroleum ether. Complex **3** was red in color, while complex **5** was dark pink. Both complexes were fully characterized using multiple analytical methods. The ^{1}H NMR spectra of both the complexes displayed peaks similar to that of the free BODIPY ligands and the mononuclear complex **1** (Fig. S2(a)). However, the peaks were shifted downfield with respect to those of the free BODIPY ligands and the mononuclear complex. This downfield shift in the proton signals might have resulted from a change in the electron density on the metal atoms after the chelation by the BODIPY ligands through their pyridine nitrogen atoms to form the desired dinuclear metal complexes. They showed two doublets at δ 8.51 and δ 7.15 and δ 8.48 and δ 7.31 which belongs to the α and β protons of the pyridyl group of the BODIPY ligands for complexes **3** and **5** respectively. The aromatic proton peaks from the avobenzone ligand appeared between δ 7.90 and δ 6.94. The spectra also contained doublets at around δ 7.79 and δ 5.68, which corresponded to the aromatic CH protons of the *p*-cymene group. Beside this they exhibited five singlets, a septet and a doublet between δ 3.85 and δ 1.24 corresponding to the methyl and methoxy protons of these complexes. The observed ^{1}H NMR peaks of these complexes were consistent with the expected products. The ESI-MS spectroscopy was carried out to further confirm the formation of the dinuclear complexes **3** and **5**. Their ESI-MS spectra obtained in acetonitrile solution exhibited prominent peaks corresponding to the loss of two triflate anions $[M\text{-}2CF_3SO_3]^{2+}$. These peaks were centered at *m/z* 784.02 and 808.02 for complexes **3** and **5**, respectively. The peaks were isotopically resolved, and matched well with its theoretical distributions (Fig. 1 and Fig. S1(c), (e)).

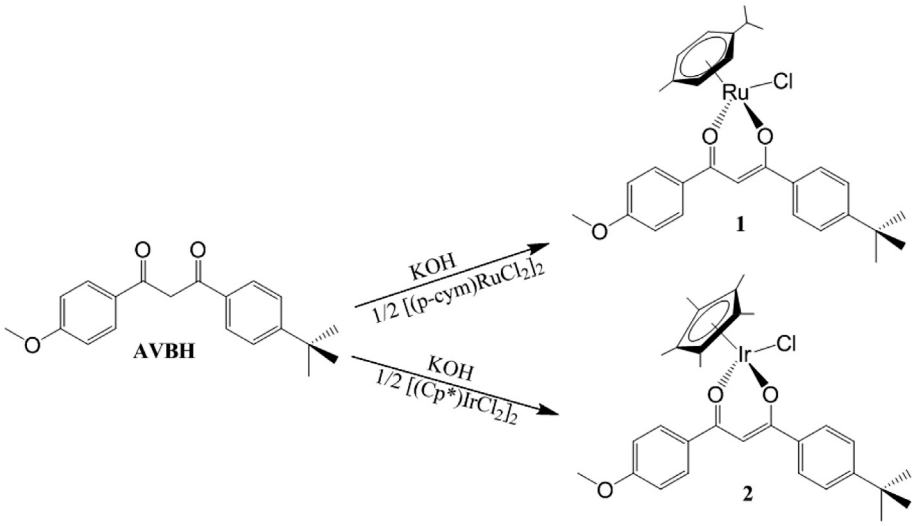

Scheme 1. Synthetic scheme for mononuclear complexes **1** and **2**. (p-cym = para-cymene).

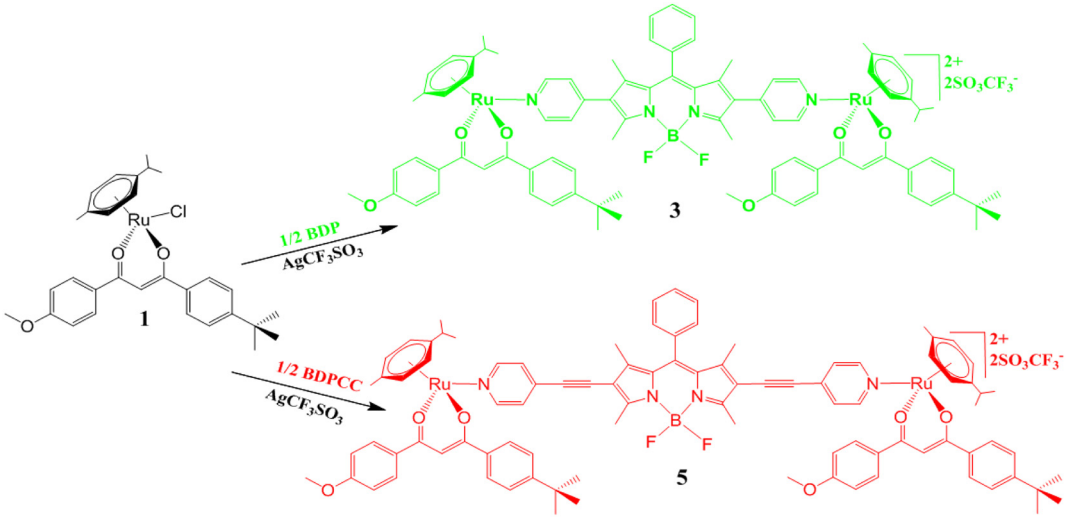

Scheme 2. Synthetic scheme for dinuclear ruthenium complexes **3** and **5.**

Similarly, the mononuclear iridium complex **2** was reacted with a half-equivalent of BDP or BDPCC in methanol to afford the cationic dinuclear complexes **4** and **6**, respectively, which were isolated as their triflate salts (Scheme 3). Compound **4** was red in color, while **6** was dark pink. The complexes were non-hygroscopic and stable in air and in solution. They were soluble in common polar solvents such as dichloromethane, chloroform, methanol, ethanol, acetone and acetonitrile but were insoluble in hexane, diethyether and petroleum ether. Both the complexes were fully characterized by different analytical methods. Like the ruthenium derivatives, the ^{1}H NMR spectra of complexes **4** and **6** were similar to those of the starting mononuclear complex **2** and the BODIPY ligands (Fig. S2(b)). The peaks were shifted downfield as compared to those of the free ligands. They displayed two doublets, at δ 8.53 and δ 7.32, and δ 8.46 and δ 7.48, which corresponded to the α and β protons of the pyridyl group of the BODIPY ligands for complexes **4** and **6**, respectively. Beside this, four doublets and a singlet between 7.97 and 6.97 ppm corresponding to the aromatic peaks of avobenzone protons are also observed. The spectra of complexes **4** and **6** also exhibited a singlet corresponding to the pentamethylcyclopentadienyl group at 1.59 and 1.61 ppm, respectively. The observed peaks were consistent with the expected products; detailed assignments of the peaks are provided in the experimental section. The ESI-MS spectra of complexes **4** and **6** in acetonitrile solution exhibited peaks corresponding to the loss of two triflate anions. These peaks were centered at *m/z* 876.12 and 900.15 for complexes **4** and **6**, respectively (Fig. S1(d), (f)).

The UV–Vis and fluorescence properties of these complexes were studied in methanol and dichloromethane solution. In methanol, the free BODIPY ligands gave rise to absorption peaks at approximately 517 nm and 555 nm for BDP and BDPCC, respectively. However, a small red shift of about 5 nm was observed when dichloromethane was used as the solvent rather than methanol. The visible region of the spectra of the BDP

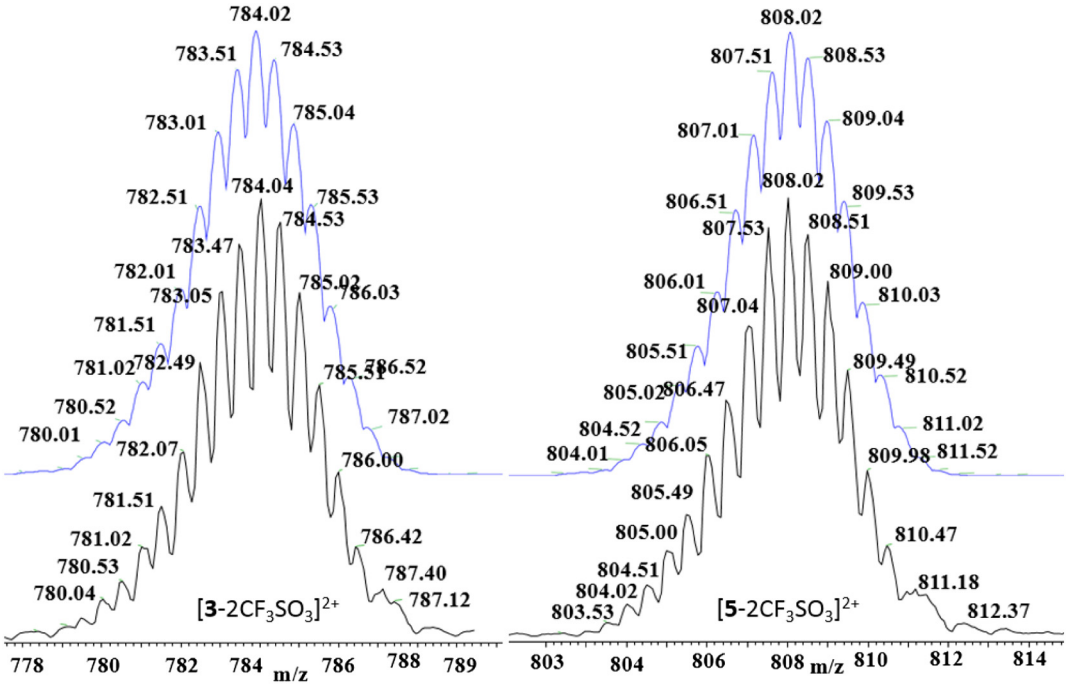

Fig. 1. ESI-MS spectra of the dinuclear complexes **3** and **5** in acetonitrile. Theoretical (blue) and experimental (black) isotopic distributions are shown for the peaks m/z = [**3**-2OTf]$^{2+}$ and m/z = [**5**-2OTf]$^{2+}$. (For interpretation of the references to color in this figure legend, the reader is referred to the web version of this article.)

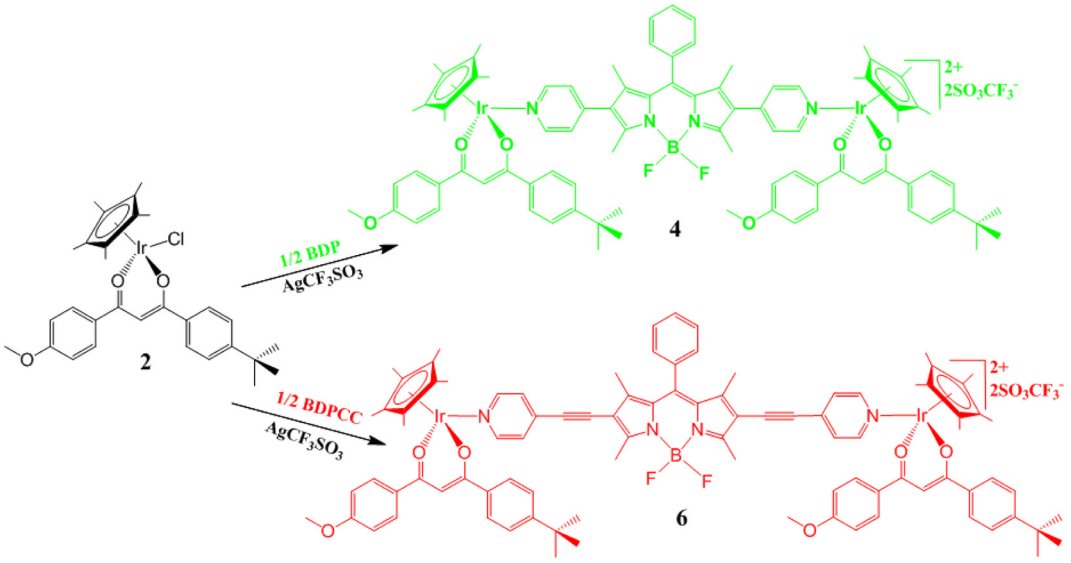

Scheme 3. Synthetic scheme for the iridium dinuclear complexes **4** and **6**.

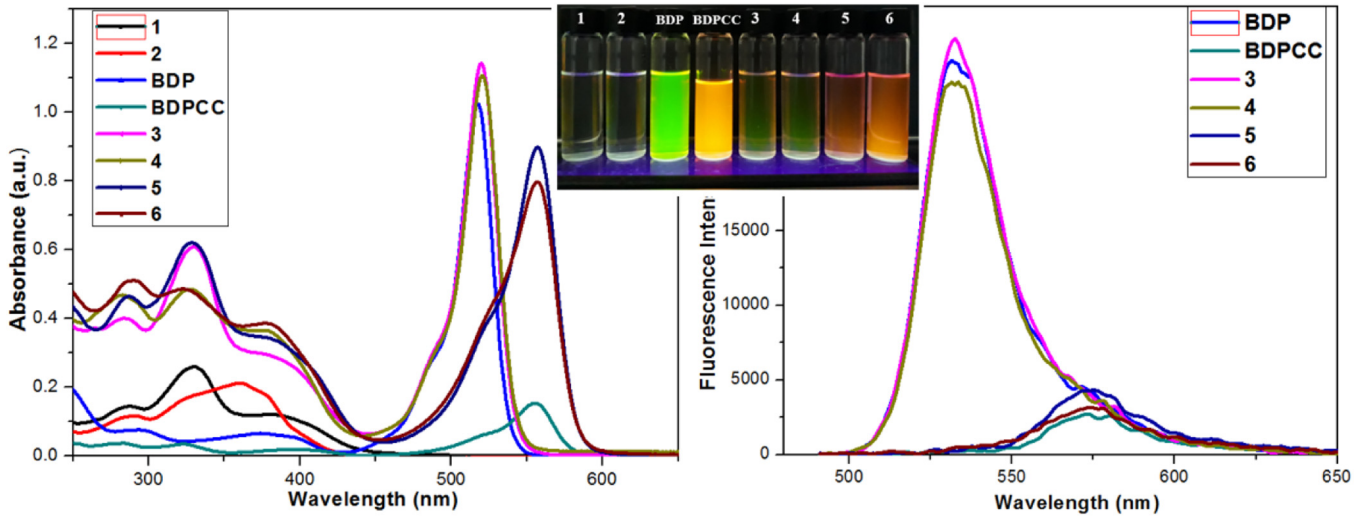

Fig. 2. Absorption (left) spectra of BDP, BDPCC, and metal complexes **1–6** in methanol, and the emission (right) spectra of BDP, BDPCC, and metal complexes **3–6** in methanol (Excitation wavelength was 480 nm). Photographic images (inset) of BDP, BDPCC, and metal complexes **1–6** in methanol under UV-light (365 nm).

based supramolecules **3** and **4** was dominated by intense peaks similar to those of free BDP. These peaks, which were centered at approximately 520 nm, were assigned to the π-π* transition arising from the BDP ligand present in these complexes. Similarly, the spectra of supramolecules **5** and **6** were dominated by intense peaks centered at 557 nm, arising from the BDPCC ligands present in these complexes. Other lower intensity peaks centered between 380 nm and 390 nm were also observed; these may arise from a combination of intra/intermolecular π-π* transitions mixed with MLCT (metal-to-ligand charge-transfer) transitions. The luminescence spectra of the BODIPY ligands and their complexes were also investigated in methanol and dichloromethane solution. The ligands and the complexes were emissive in solution, and their spectra exhibited emission bands centered at 532 nm and 575 nm, arising from the BDP and BDPCC groups present in these complexes, respectively. These complexes gave rise to similar absorption spectra, in agreement with the UV–visible spectrum of the free BODIPY ligands. The absorption and emission spectra are shown in Fig. 2.

2.2. DFT calculations

Our repeated efforts to grow single crystals of these complexes were not successful. Therefore, in order to gain insight into the molecular structures of the BODIPY-based organometallic complexes **3–6**, we carried out a computational study based on density functional theory (DFT). The structures of the complexes were optimized using the ωB97X-D functional [13a] and 6-31G(d) basis set implemented in the Gaussian09 software package [13b], which were recently applied to describe the formation of complicated Ru(II) organometallic complexes, Borromean ring [13c] and Solomon link [13d]. For the Ru and Ir atoms, the LanL2DZ effective pseudo-potential and corresponding basis set were used for all the calculations [13e]. The polarizable continuum model (PCM) using the integral equation formalism variant (IEFPCM) was employed to reflect the influence of the solvent medium used in the syntheses of these complexes (i.e., for methanol, $\varepsilon = 32.613$) [13f].

The local minimum structures of Ru(II) complexes **3** and **5** are presented in Fig. 3. The relative energies of the local minimum structures are within only ~1 kcal/mol (Table S1). For the case of Ir(III) complexes **4** and **6**, nearly identical results were observed (Table S1 and Fig. S4(a)). Therefore, our computational results suggest that the relative stability of the isolated organometallic complexes did not depend strongly on the orientation of the side functional groups and could not be determined at this level of DFT. The influence of the orientation of

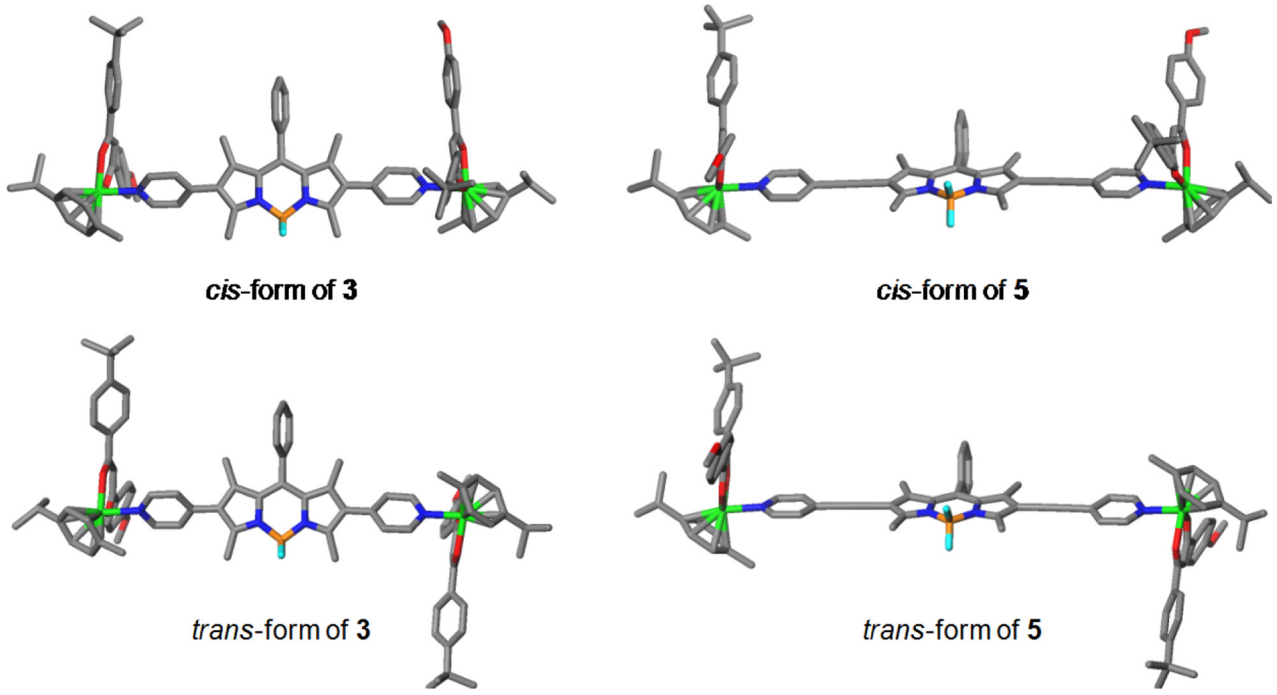

Fig. 3. Optimized structures of the *cis*- and *trans*-forms of the dinuclear organometallic complexes **3** and **5**. (Ru, green; F, sky-blue; O, red; N, blue; C, gray; B, orange; H atoms are omitted for clarity.) (For interpretation of the references to color in this figure legend, the reader is referred to the web version of this article.)

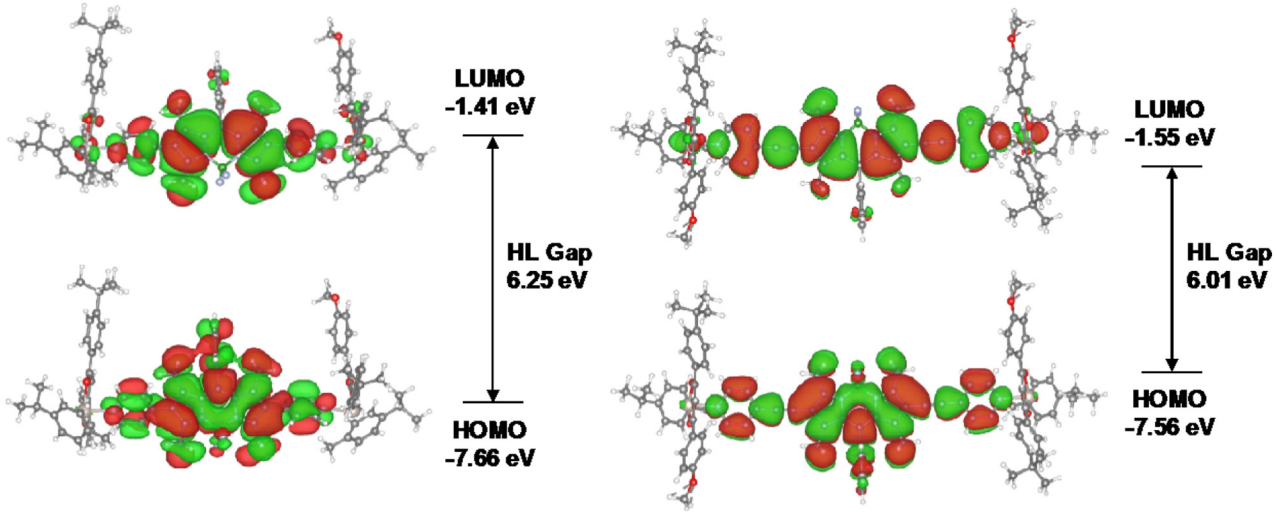

Fig. 4. Highest occupied and lowest unoccupied molecular orbitals (HOMO and LUMO) of the *cis*-forms of **3** and **5**.

the side functional groups on the frontier electronic structures of Ru(II) complexes was also insignificant, because the highest occupied and lowest unoccupied molecular orbitals (HOMO and LUMO) were mainly distributed on the BDP and BDPCC ligands for **3** and **5**, respectively, as shown in Fig. 4. Not only the HOMO and LUMO for the *trans*-form of **3** and **5** are similar to those of their *cis*-form (Fig. S4(b)) but also Ir(III) complexes exhibited the identical spatial distributions of HOMO and LUMO (Fig. S4(c), S4(d)). Based on our experimental and theoretical studies, we ruled out the formation of any isomers in our complexes. The computationally obtained frontier molecular orbitals provided a reasonable insight into the optical properties of organometallic complexes. The energy gaps between HOMO and LUMO (HL gaps) of **3** and **4** with BDP and **5** and **6** with BDPCC were ~6.25 and ~6.01 eV, respectively (Table S1). These values were consistent with the absorption spectra which were dominated by the intramolecular π-π* transition (Fig. 2). The extension of the π-conjugated network of BDP due to the presence of ethynyl group reduced the HL gap. Therefore, our computational results indicated that the optical properties of organometallic complexes containing BODIPY-based ligand can be finely tuned by adjusting the length of π-conjugated network around the BODIPY ligand.

2.3. Biological studies

2.3.1. MTT (3-(4,5-dimethylthiazol-2-yl)-2,5-diphenyltetrazolium bromide) assays

Considering the increasing importance of ruthenium and iridium complexes as anticancer agents, the anticancer activity of free avobenzone and complexes **1–6** was studied against the human cancer cell lines A549 (lung cancer), HeLa (cervical cancer) and MCF-7 (breast cancer) as well as a non-malignant NIH T3T cells (mouse embryo fibroblast) cell line. They exhibited moderate to high activity, ranging

Table 1
In vitro antiproliferative activity (IC_{50} in μM) of free AVBH, complexes **1**–**6**, and doxorubicin on cancerous (A549, Hela, MCF-7) and non-cancerous (NIH 3 T3) cell lines.

Complexes	NIH 3T3	A549	Hela	MCF-7
AVBH	3.0 ± 0.3	5.0 ± 0.8	4.0 ± 0.8	3.0 ± 0.5
1	3.0 ± 0.4	4.0 ± 0.6	3.0 ± 0.4	4.0 ± 0.6
2	4.0 ± 0.6	5.0 ± 0.8	4.0 ± 0.6	4.0 ± 0.7
3	4.0 ± 0.7	4.0 ± 0.5	4.0 ± 0.7	5.0 ± 0.8
4	5.0 ± 1.4	4.0 ± 0.4	4.0 ± 0.6	3.0 ± 0.4
5	2.0 ± 0.5	3.0 ± 0.7	3.0 ± 0.7	1.8 ± 0.6
6	1.0 ± 0.8	3.0 ± 0.4	2.0 ± 0.3	1.3 ± 0.3
Doxorubicin	1.7 ± 0.2	1.5 ± 0.6	1.4 ± 0.4	1.0 ± 0.9

from 1 to 5 μM. The results are summarized in Table 1. Among the tested compounds, ruthenium complex **5** and iridium complex **6** featuring the BDPCC ligand exhibited the highest cytotoxic activity against MCF-7, with IC_{50} values of 1.8 ± 0.6 and 1.3 ± 0.3 μM, respectively. The extent of toxicity in non-malignant NIH T3T cells however, was more or less comparable with the other cell lines, thus ruling out the possibility of any selectivity towards cancer cell killing. In contrast, the control molecule doxorubicin showed the lowest cytotoxicity in all cells. The free BODIPY ligands were previously found to be non-toxic [9f,12a,12g].

2.4. DNA binding studies

2.4.1. UV–visible spectroscopic study

To determine how these small molecules interact with DNA, detailed binding assays were carried out using UV–visible spectroscopy. Upon the addition of Calf-Thymus-DNA (CT-DNA) to solutions of complexes **5** and **6,** the characteristic peak observed at 572 nm exhibited concentration-dependent hyperchromic shift (Fig. 5). No isosbestic point was observed upon the interaction of complexes **5** or **6** with the CT-DNA. The hyperchromicity of the absorption band upon the addition of CT-DNA indicated that supramolecules **5** and **6** interacted with the CT-DNA and damaged its double helical structure [14]. Based on the absorbance values obtained, the **5/6** CT-DNA ***dissociation constants*** (K_d) was calculated. The K_d values obtained for the interaction of **5** and **6** with CT-DNA were 180 μM and 132 μM, respectively. The results indicated that CT-DNA interacted more strongly with the ruthenium complex **5** than with the iridium complex **6**. Nevertheless, UV–visible titration studies alone were not sufficient to fully characterize the CT-DNA-**5/6** interaction. To determine the binding mode and the extend of the interaction between CT-DNA and **5/6**, additional spectroscopic studies were carried out.

2.5. Fluorescence titration studies

Since the supramolecules 5 and 6 were fluorescent, their interaction with CT-DNA could be monitored using fluorescence spectroscopy. The interaction of CT-DNA with 5 and 6 gave rise to an emission peak at around 601 nm that exhibited hyperchromicity. As an interacting fluorescent molecule approaches the DNA bases, the exchange of fluorescent energy from the fluorescent molecule and adjacent DNA bases increases the intensity of the fluorescence emission signal [15]. The only way in which 5 and 6 could approach the DNA bases is by insertion between two stacked base pairs. Therefore, these results indicated that the supramolecules 5 and 6 may intercalate into the bases of CT-DNA. The fluorescence spectra obtained during the interaction of CT-DNA with supramolecules 5 and 6 are shown in Fig. 6.

2.6. Circular dichroism studies

The UV–visible and fluorescence spectroscopy studies indicated that complexes 5 and 6 may possibly intercalate into CT-DNA. In order to further understand the effect of complexes 5 and 6 on the conformation of CT-DNA, circular dichroism (CD) studies were performed. The CT-DNA showed positive and negative CD bands at around 270 nm and 240 nm, respectively. Upon the addition of 15 μM of 5 and 6 to CT-DNA, the positive CD band intensity decreased, indicating unwinding of CT-DNA [16]. Further, upon doubling the concentration of 5 and 6 (to a 1:2 ratio), the positive band intensity decreased further, suggesting that at higher concentrations of 5 and 6, the melting of CT-DNA increased. A greater decrease in the intensity of CD band was noted for complex 6 than for complex 5. These results indicate that the interactions of complexes 5 and 6 with CT- DNA caused the CT- DNA structure to unwind gradually. The CD spectra of supramolecules 5 and 6 with CT-DNA are shown in Fig. 7.

2.7. Flow cytometry experiments

2.7.1. Cell cycle assay

The results obtained from the MTT assays indicated that among the complexes studied, complexes **5** and **6** exhibited the highest cytotoxicity in the studied cancer cell lines. To better understand the role of these complexes in cells and to identify a possible cause for the higher cytotoxicity and efficacy of complexes **5** and **6** in the cancer cell lines, cell cycle assays and apoptotic assays were performed using flow cytometry in the presence and absence of the complexes at their respective IC_{50} values. The results of these experiments suggested that complexes **5** and **6** inhibit the cell cycle at the subG1 stage. It has been previously reported that subG1 phase arrest can enhance cytotoxicity and induce apoptosis in cells [17]. Among the complexes studied, the greatest subG1 phase inhibition values were observed for 5 μM and 1 μM of complex **6** (14.67% and 11.67%, respectively), followed by

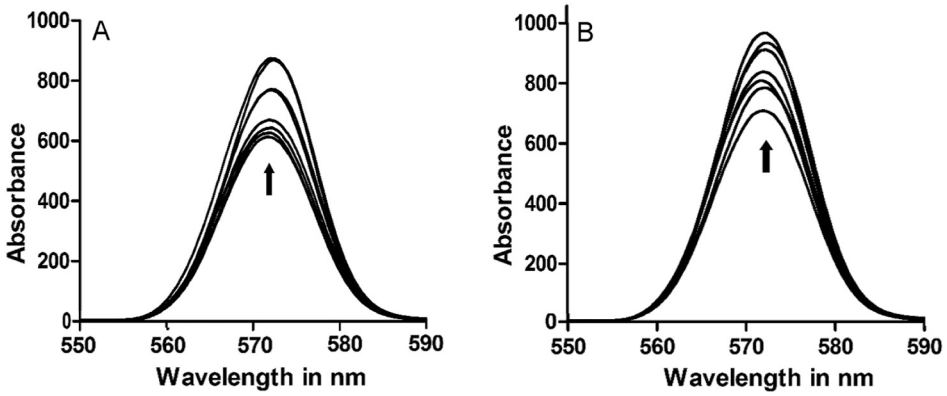

Fig. 5. UV–vis absorption spectra indicating the binding interaction between complexes **5** (A), **6** (B) and CT DNA. UV–vis spectra of complexes **5** and **6** (2.5 μM) obtained upon the addition with increments of 0.05 μM CT DNA are shown. (A) UV–vis spectra obtained when CT DNA in 100 mM TE (pH 7.0) was added to complex **5** at 20 °C. (B) UV–vis spectra obtained when CT DNA in 100 mM TE (pH 7.0) was added to complex **6** at 20 °C. The arrows indicate the direction in which the absorption peak moves after interaction of complexes **5** and **6** with CT DNA.

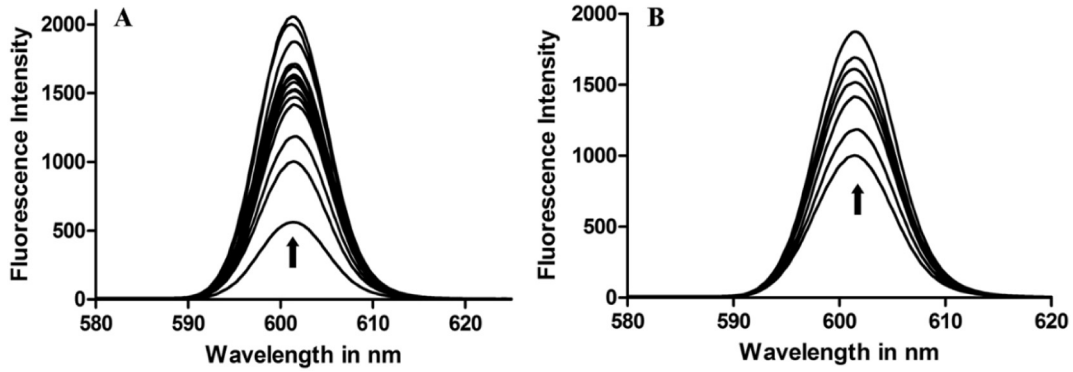

Fig. 6. Fluorescence spectroscopic titration of complexes **5** (A), **6** (B) with CT DNA. Fluorescence spectra of complexes **5** and **6** (10 μM) is recorded on the addition with increments of 0.005 μM CT DNA are shown. (A) Fluorescence spectra obtained when the CT DNA in 100 mM TE (pH 7.0) was added to 10 μM of complex **5** at 20 °C. (B) Fluorescence spectra obtained when the CT DNA in 100 mM TE (pH 7.0) was added to 10 μM of complex **6** at 20 °C. The arrows indicate the direction in which the fluorescence peak moves upon addition of CT DNA to the solution of complexes **5** and **6**.

complex **5** (10.08%), while the untreated MCF-7 cells showed a subG1 phase inhibition of only 5.10%. These results confirmed that both complexes induced cytotoxicity followed by apoptosis in the cancer cell lines through subG1 phase arrest. The details of the cell cycle assays are presented in Fig. 8 and documented in Table 2.

2.7.2. Apoptosis assay

From the apoptosis assays, it was clear that 5 μM of complex 6 had a higher potential to induce apoptosis (11.86%) in MCF-7 cells than a similar concentration of complex 5 (7.81%). The results also indicated that complex 6 (at 1 μM) was effective at inducing a higher proportion of apoptotic cells [6.45% late apoptotic cells (Annexin-V + /PI +) and 2.62% early apoptotic cells (Annexin-V + /PI −)] in MCF-7 cells. Upon treating the cells with a higher concentration of complex 6 (5 μM) a higher percentage of apoptotic cells were observed [7.65% late apoptotic cells (Annexin-V + /PI +) and 4.21% early apoptotic cells (Annexin-V + /PI −)]. However, when MCF-7 cells were treated with 5 μM complex 5, fewer apoptotic cells were observed (7.81%) than with complex 6, indicating the greater potential of complex 6 to induce apoptosis in human breast cancer cells. The results obtained from the apoptosis assay supported those of the MTT assay. The percentages of cell population in viable, necrotic, and early or late apoptotic phases are shown in Table 3. The results from the apoptosis assay for untreated MCF-7 cells and cells treated with 1 μM and 5 μM of complexes 5 and 6 are depicted in Fig. 9.

2.7.3. Fluorescence microscopy study

Induction of apoptosis among cancer cells occurs due to multiple causes. In the majority of cases, the primary feature observed upon the onset of apoptosis is the fragmentation of nuclear DNA and chromatin condensation [18]. Several apoptotic cells with condensed and fragmented DNA were observed upon treating the cells with 1 μM of complexes 5 and 6. When the concentration of 5 and 6 was further increased to 5 μM, the number of apoptotic cells also increased. A significant increase in the percentage of cells with condensed and fragmented DNA (apoptotic cells) occurred when the concentrations of 5 and 6 were increased from 1 μM to 5 μM (Fig. 10). The cells with condensed DNA can be seen as bright blue spots in the microscopy images. They are marked with white arrows in Fig. 10. Several previous studies emphasized that the majority of synthetic small molecules, such as doxorubicin [19], mitoxantrone [20], acridine orange [21], exhibit anticancer activity through dsDNA intercalation [22]. We speculate that the possible intercalation of 5 and 6 with dsDNA is a possible reason for the potential anticancer activity of 5 and 6.

2.7.4. Mitochondrial outer membrane permeability

Binding studies so far, indicate that complexes **5** and **6** are capable of interacting with DNA. Furthermore, flow cytometry and fluorescence microscopy experiments, exhibit their potential to induce apoptosis among MCF-7 cells. Therefore, it becomes interesting to understand their effects on mitochondria, as thus have an insight on their mechanistic side. Alteration in mitochondrial outer membrane permeability is assessed using Mitotracker red staining. The MCF-7 cells before and after the treatment with complexes **5** and **6** are labeled with Mitotracker red. It is evidenced that mitochondria were evenly distributed in the cytosol of untreated cells (see Fig. 11), where about 10–15 mitochondria were seen in the cytosol. Moreover, the untreated MCF-7 cells (control) showed freely distributed mitochondria in the cytosol. However, upon treatment with 5 μM of the complexes, aggregations of mitochondria were observed (the aggregated

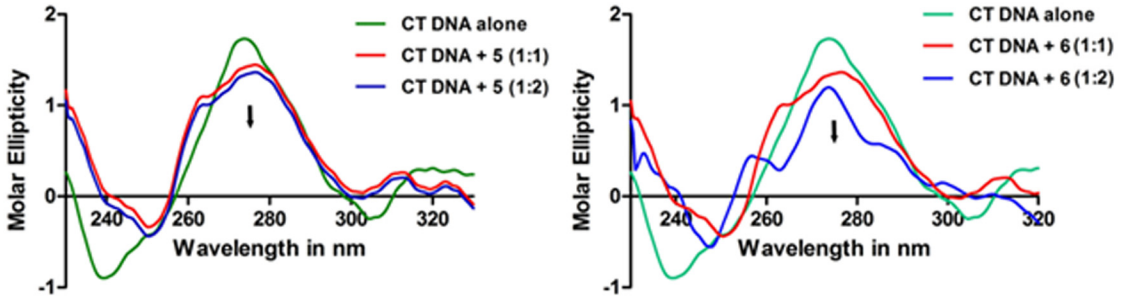

Fig. 7. Circular dichroism studies illustrating the changes in the CT-DNA conformation upon interaction with complexes **5** (left) and **6** (right). (A) CD spectra obtained with the CT-DNA in 100 mM TE (pH 7.0) at 20 °C and upon addition of 1:1 and 1:2 ratios of CT-DNA and complex **5** (B) CD spectra obtained with the CT-DNA in 100 mM TE (pH 7.0) at 20 °C and upon addition of 1:1 and 1:2 ratios of CT-DNA and complex **6**. CD spectra were averaged over three scans. The arrows indicate the direction of movement of CD peaks upon addition of complexes **5** and **6**.

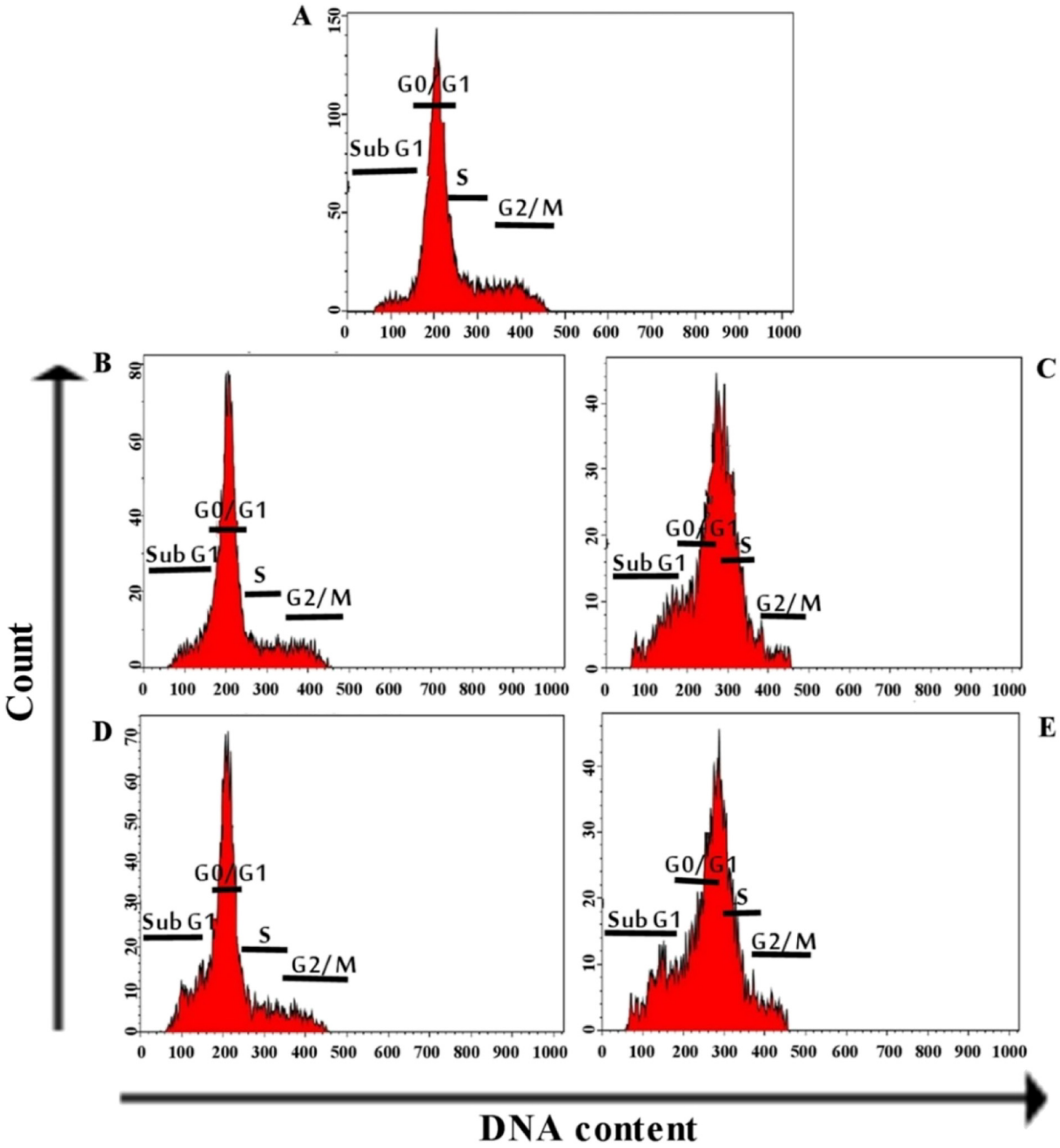

Fig. 8. Cell cycle studies indicating the effect of complexes **5** and **6** on cell cycle progression (A) MCF-7 cells without the addition of any complex (control MCF-7 cells) (B) MCF-7 cells treated with 1 μM of complex **5** for 48 h (C) MCF-7 cells treated with 5 μM complex of **5** for 48 h (D) MCF-7 cells treated with 1 μM of complex **6** for 48 h (E) MCF-7 cells treated with 5 μM of complex **6** for 48 h.

Table 2
Data obtained from cell cycle histograms indicating the percentage of cells in each phase of the cell cycle before and after treatment with complexes **5** and **6**.

S. No.	Complexes	Sub G_1	G0/G_1	G_2/M	S
1	**Control**	05.10%	70.47%	10.72%	13.63%
2	**5** (1 μM)	09.28%	57.78%	08.81%	18.90%
3	**6** (1 μM)	11.67%	22.84%	10.95%	54.10%
4	**5** (5 μM)	10.08%	67.74%	07.01%	12.19%
5	**6** (5 μM)	14.67%	64.55%	07.88%	12.48%

mitochondria are marked with white arrows). The aggregation of mitochondria was reported to occur, when cells enter into apoptosis [23], and accordingly leading to the release of cytochrome *c* into the cytosol, which in turn triggered the cascade pathway to apoptosis. From Fig. 11, it was clear that mitochondria were getting bundled with complexes **5** and **6**, indicating the onset of apoptosis in MCF-7 cells.

3. Conclusions

In conclusion, we have designed new ruthenium and iridium metal complexes based on the sunscreen agent avobenzone and fluorescent BODIPY ligands. The complexes were fully characterized using multiple analytical techniques, and their structures were further rationalized by density functional theory studies. In light of the growing interest of the use of metal-based complexes in biological systems, the anticancer properties of the synthesized complexes were studied in detail. The BDPCC based complexes 5 and 6 were found to be more cytotoxic than

Table 3
Data obtained from dot plots indicating the percentage of viable and apoptotic cells before and after treatment with complexes **5** and **6**.

S. No.	Samples	Percentage of Viable Cells (LL)	Percentage of Necrotic Cells (UL)	Percentage of apoptotic cells	
				UR	LR
1	**Control**	99.84	00.02	00.07	00.07
2	**5** (1 μM)	96.01	00.05	00.18	03.76
3	**5** (5 μM)	88.08	04.11	05.08	02.73
4	**6** (1 μM)	90.18	00.75	06.45	02.62
5	**6** (5 μM)	81.24	07.09	07.65	04.21

LL: lower left quadrant of the dot plot; UL: upper right quadrant of the dot plot; LR: lower right quadrant of the dot plot; UR: upper right quadrant of the dot plot.

the BDP compounds 3 and 4, with their activity comparable to that of the chemotherapy drug doxorubicin. These complexes were also found to bind strongly with genomic DNA causing the unwinding of the double helix, where complex 6 showed a comparatively better activity. Complex 6, also showed better affinity to instigate apoptosis in breast cancer cells than 5, which was further confirmed by Annexin V/PI apoptosis and fluorescent microscopy studies. To further understand its mechanism, in-depth studies of these complexes in animal models are being performed in our laboratory.

4. Experimental section

4.1. General information

The dipyridine bodipy ligands were synthesized by our previously reported methods.[9f, 12g] The starting dimers $[(\eta\ 6\text{-}p\text{-cymRu})Cl_2]_2$ and

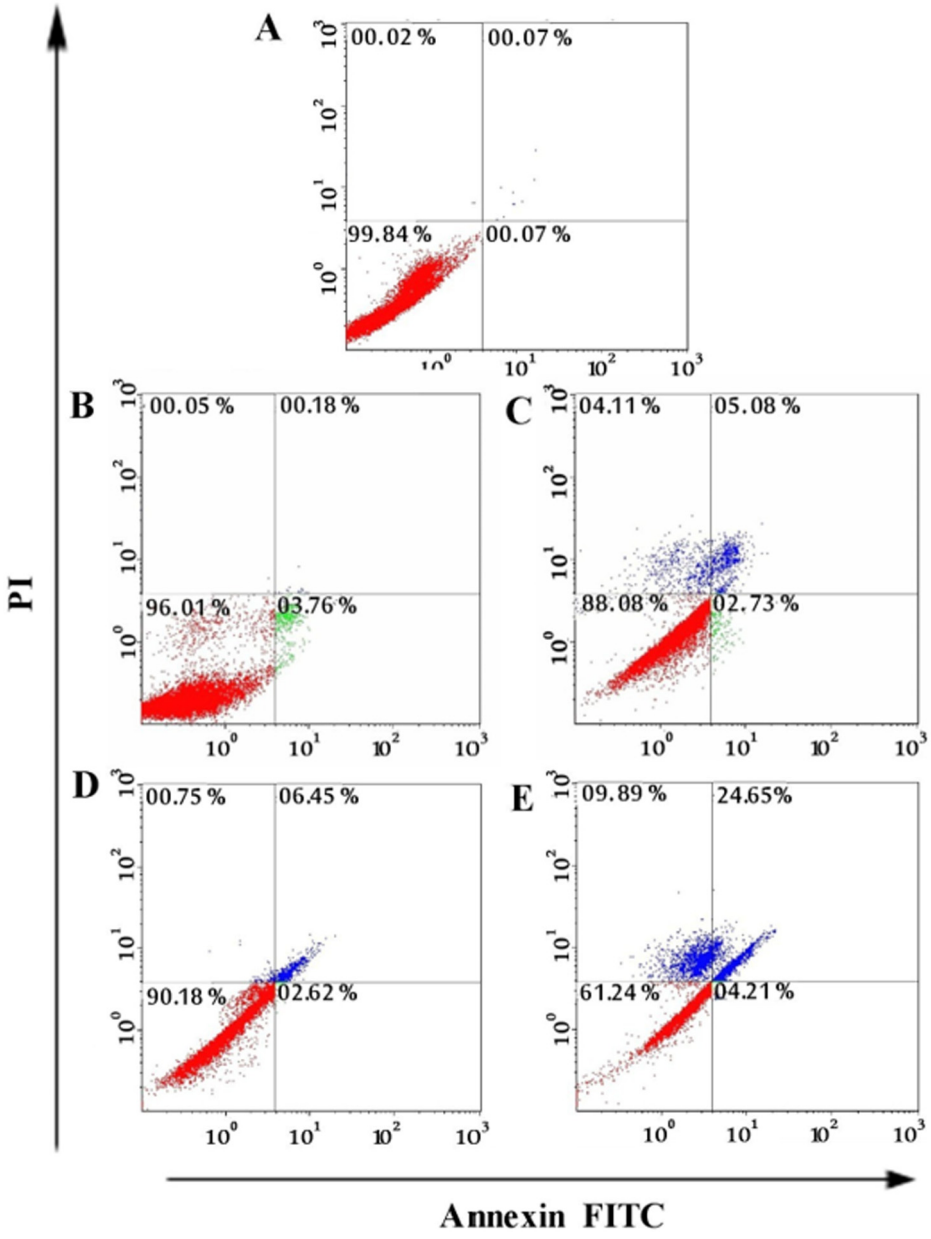

Fig. 9. Annexin V-FITC vs propidium iodide plots (dot plots) obtained from the gated cells show the population of cells corresponding to viable, early, and late apoptotic and necrotic cells. (A) MCF-7 cells without the addition of any complex (control MCF-7 cells) (B) MCF-7 cells treated with 1 μM of complex **5** for 24 h (C) MCF-7 cells treated with 5 μM of complex **5** for 24 h (D) MCF-7 cells treated with 1 μM of complex **6** for 24 h (E) MCF-7 cells treated with 5 μM of complex **6** for 24 h.

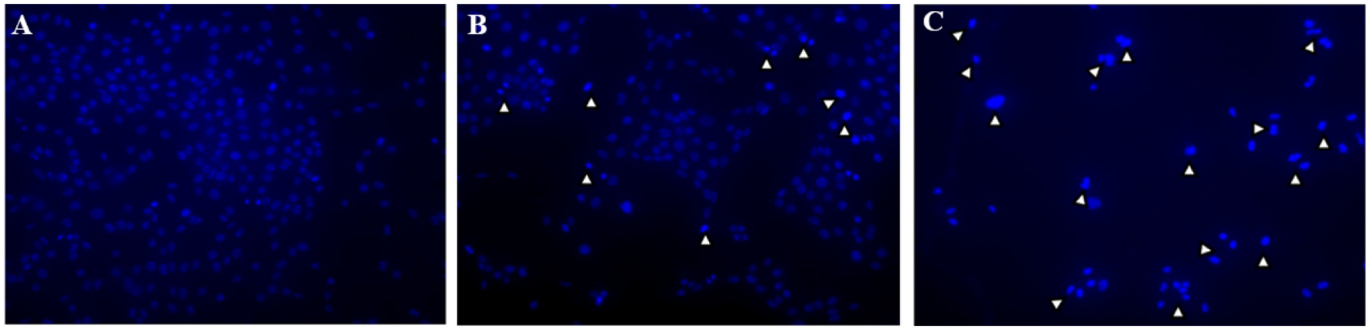

Fig. 10. Confocal microscopy images showing variation in the morphology of cells among normal and apoptosis-induced MCF-7 cells upon staining with Hoechst 33258 and MCF-7 cells. MCF-7 cells were treated with complexes **5** and **6** for 48 h (A) Untreated MCF-7 cells (control) do not show chromatin condensation (B) MCF-7 cells treated with 5 μM of complex **5** (C) MCF-7 cells treated with 5 μM of complex **6**. The condensed chromatin after Hoechst 33258 labeling can be seen as a bright blue spot under the fluorescence microscope. The white arrows point to the apoptotic cells that are bright blue in color. (For interpretation of the references to color in this figure legend, the reader is referred to the web version of this article.)

$[(\eta\ 5\text{-}C_5Me_5Ir)Cl_2]_2$ were purchased from Aldrich and avobenzone was purchased from TCI Korea and used as received. Dry solvents were purchased from Aldrich and all other reagents were commercially available and used without further purification. The ^1H, $^{13}C\{^1H\}$ and ^{19}F NMR spectra were recorded on an Agilent 400-MR spectrometer using the residual protonated solvent as internal standard. Infrared spectra were recorded on a Bruker/Hyperion 2000 FTIR spectrometer using KBr pellets. UV–visible absorption spectra were recorded on a Thermo Scientific Genesys 10S UV–Vis spectrometer. Fluorescence spectra were recorded on a Scinco FluoroMate FS-2 fluorescence spectrometer. ESI-MS were recorded on a Waters SynaptG2*Si* spectrometer at KBSI, South Korea. Elemental analysis was recorded on an Elemental Analyzer (Elementar Analysensysteme GmbH, Germany) at KBSI, Korea.

4.2. General synthesis

Synthesis of complex 1 and 2: Complex 1 was synthesized by following a recently reported method [11a]. KOH (21 mg, 0.374 mmol) was added to a solution of avobenzone (116 mg, 0.374 mmol) dissolved in dry methanol (10 mL). The mixture was stirred for around 1 h at room temperature followed by the addition of $[(\eta\ 6\text{-}p\text{-cymRu})Cl_2]_2$ (104 mg, 0.169 mmol, for complex 1) and $[(\eta\ 5\text{-}C_5Me_5Ir)Cl_2]_2$ (135 mg, 0.169 mmol, for complex 2). The mixture was stirred for 24 h at room temperature. The orange or yellow precipitate formed was centrifuged and washed several times with hexane and recrystallized in dichloromethane. Then the solid was dried under vacuum.

4.2.1. Complex 1

4.2.1.1. Orange solid. Yield 156 mg (79%). ESI-MS (CH_3CN): *m/z* = 545.14 $[M - Cl]^+$. IR (KBr pellets): ν = 2960 (m, C—H); 1608, 1588, 1528 (s, C═O, C═C). Anal. calcd for $C_{30}H_{35}O_3ClRu{\cdot}CH_2Cl_2$: C, 55.99; H, 5.61. Found: C, 55.69; H, 5.44. ^1H NMR (400 MHz, Acetone-d_6): δ = 8.00 (d, 2H, J = 8 Hz, H_a), 7.93 (d, 2H, J = 8 Hz, H_b), 7.47 (d, 2H, J = 8 Hz, H_c), 6.97 (d, 2H, J = 8 Hz, H_d), 6.47 (s, 1H, H_e), 5.70 (d, 2H, J = 8 Hz, H_{cym}), 5.39 (d, 2H, J = 8 Hz, H_{cym}), 3.85 (s, 3H, $OCH_{3,\ AVB}$), 3.00 (m, 1H, $CH(CH_3)_2$), 2.28 (s, 3H, $CH_{3,cym}$), 1.41 (d, 6H, J = *4* Hz, $CH(CH_3)_2$), 1.33 (s, 9H, $(CH_3)_{3,\ AVB}$). $^{13}C\{^1H\}$-NMR (100 MHz, Acetone-d_6): δ = 180.19, 180.00, 161.78, 153.92, 136.62, 131.50, 129.01, 126.90, 125.09, 113.32, 98.79, 96.97, 91.36, 83.59, 79.19, 54.91, 34.41, 30.48, 21.75, 17.10.

4.2.2. Complex 2

4.2.2.1. Yellow solid. Yield 175 mg (76%). ESI-MS (CH_3CN): *m/z* = 637.13 $[M - Cl]^+$. IR (KBr pellets): ν = 2966 (m, C—H); 1580, 1525 (s, C═O, C═C). Anal. calcd for $C_{30}H_{35}O_3ClIr$: C, 53.60; H, 5.40. Found: C, 53.29; H, 5.43. ^1H NMR (400 MHz, Acetone-d_6): δ = 8.04 (d, 2H, J = 8 Hz, H_a), 7.97 (d, 2H, J = 8 Hz, H_b), 7.48 (d, 2H, J = 8 Hz, H_c), 6.98 (d, 2H, J = 8 Hz, H_d), 6.58 (s, 1H, H_e), 3.86 (s, 3H, $OCH_{3,\ AVB}$), 1.66 (s, 15H, cp*), 1.33 (s, 9H, $(CH_3)_{3,\ AVB}$). $^{13}C\{^1H\}$-NMR (100 MHz, Acetone-d_6): δ = 179.48, 178.78, 162.92, 152.24, 135.44, 131.99, 129.66, 127.60, 126.02, 114.40, 93.56, 84.15, 55.74, 35.40, 31.36, 8.84.

Synthesis of complexes 3 and 5: Compound 1 (30 mg, 0.051 mmol) was dissolved in methanol (20 mL) and $AgCF_3SO_3$ (15 mg, 0.058 mmol) was added to the solution. The reaction mixture was stirred for 1 h at room temperature and filtered to remove AgCl formed. BODIPY (12.5 mg, 0.26 mmol for BDP, 3 and 13.7 mg, 0.26 mmol for BDPCC, 5) was then added to the filtrate and dry nitrogen was bubbled for 10–15 min. The resulting mixture was then stirred for 24 h at room

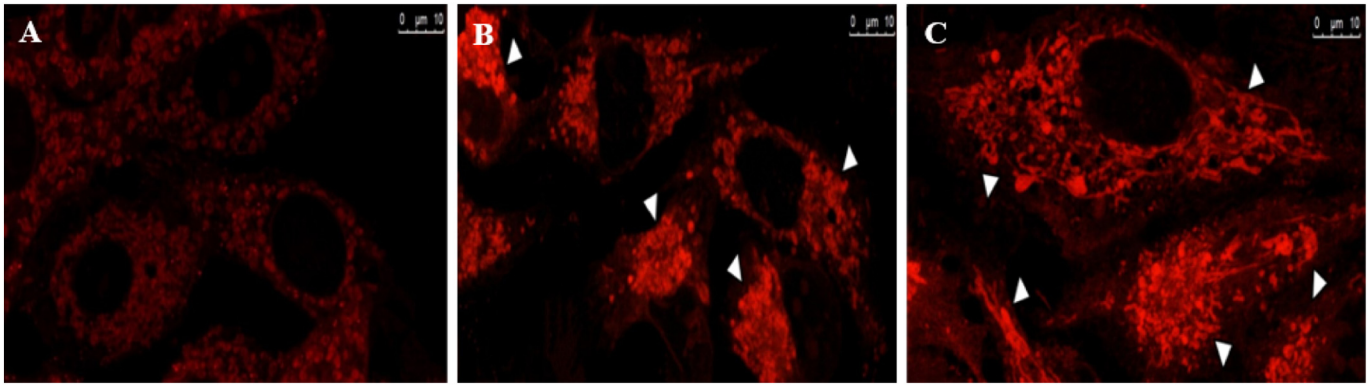

Fig. 11. Mitochondrial aggregation among MCF-7 cells before and after the treatment with 5 μM of complexes **5** and **6** (white arrows show aggregation of mitochondria), A-mitochondria before complex treatment, B-mitochondria after treatment with complex **5** and C-mitochondria after treatment with complex **6**.

temperature. The solution was reduced to 3 mL and an excess of hexane was slowly layered and kept in refrigerator. The precipitate formed was collected by centrifugation, washed several times with hexane, recrystallized in chloroform and dried in vacuum.

Complex 3: Red solid. Yield 35 mg (73%). ESI-MS (CH_3CN): *m/z* = 784.02 $[M - 2CF_3SO_3]^{2+}$. IR (KBr pellets): ν = 2968 (m, C−H); 1598, 1523 (s, C═O, C═C); 1249 (s, CF_3). Anal. calcd for $C_{91}H_{95}O_{12}Ru_2N_4BF_8S_2{\cdot}5.5CHCl_3$: C, 45.95; H, 4.02; N, 2.22. Found: C, 46.35; H, 4.03; N, 2.29. ^{1}H NMR (400 MHz, $CDCl_3$): δ = 8.51 (d, 4H, *J* = 4 Hz, H_α), 7.89 (d, 4H, *J* = 8 Hz, H_a), 7.81 (d, 4H, *J* = 8 Hz, H_b), 7.45 (d, *J* = 8, 4H, H_c, + 3H, H_{Ph}), 7.24 (m, 2H, H_{Ph}), 7.15 (d, 4H, *J* = 8 Hz, H_β), 6.94 (d, 4H, *J* = 8 Hz, H_d), 6.29 (s, 2H, H_e), 5.79 (d, 4H, *J* = 4 Hz, H_{cym}), 5.68 (d, 4H, *J* = 8 Hz, H_{cym}), 3.85 (s, 6H, $OCH_{3,\ AVB}$), 2.87 (sept, 2H, *J* = 8 Hz, $CH(CH_3)_2$), 2.43 (s, 6H, $CH_{3,BDP}$), 2.19 (s, 6H, $CH_{3,cym}$), 1.32 (br, 12H, $CH(CH_3)_2$) + 18H, $(CH_3)_{3,\ AVB}$), 1.24 (s, 6H, $CH_{3,BDP}$). ^{13}C{^{1}H}-NMR (100 MHz, Acetone-d_6): δ = 180.44, 180.42, 162.55, 154.73, 151.68, 150.58, 144.07, 134.83, 133.65, 132.92, 131.07, 129.60, 129.19, 129.11, 129.09, 129.00, 128.98, 127.35, 126.75, 126.14, 124.99, 113.31, 102.36, 98.60, 91.61, 83.77, 81.84, 54.54, 34.14, 30.20, 29.98, 21.19, 16.26, 11.72. ^{19}F NMR (376 MHz, $CDCl_3$): δ = −78.12 (s, 6F, $F_{C\text{-}F}$), −145.48 (q, 2F, $F_{B\text{-}F}$).

Complex 5: Red solid. Yield 25 mg (58%). ESI-MS (CH_3CN): *m/z* = 808.02 $[M - 2CF_3SO_3]^{2+}$. IR (KBr pellets): ν = 2966 (m, C−H); 2205 (m, C≡C); 1611, 1517 (s, C═O, C═C); 1249 (s, CF_3). Anal. calcd for $C_{95}H_{95}O_{12}Ru_2N_4BF_8S_2{\cdot}5CHCl_3$: C, 47.84; H, 4.01; N, 2.23. Found: C, 48.10; H, 4.05; N, 2.23. ^{1}H NMR (400 MHz, $CDCl_3$): δ = 8.48 (d, 4H, *J* = 4 Hz, H_α), 7.90 (d, 4H, *J* = 8 Hz, H_a), 7.81 (d, 4H, *J* = 8 Hz, H_b), 7.51 (m, 3H, H_{Ph}), 7.46 (d, 4H, *J* = 8 Hz, H_c), 7.31 (d, 4H, *J* = 4 Hz, H_β), 7.20 (m, 2H, H_{Ph}), 6.94 (d, 4H, *J* = 8 Hz, H_d), 6.39 (s, 2H, H_e), 5.81 (d, 2H, *J* = 8 Hz, H_{cym}), 5.76 (d, 2H, *J* = 4 Hz, H_{cym}), 5.68 (d, 4H, *J* = 8 Hz, H_{cym}), 3.85 (s, 6H, $OCH_{3,\ AVB}$), 2.84 (sept, 2H, *J* = 8 Hz, CH $(CH_3)_2$), 2.59 (s, 6H, $CH_{3,\ BDP}$), 2.18 (s, 6H, $CH_{3,\ cym}$), 1.48 (s, 6H, $CH_{3,\ BDP}$), 1.32 (m, 12H, $CH(CH_3)_2$, + 18H, $(CH_3)_{3,\ AVB}$). ^{13}C{^{1}H}-NMR (100 MHz, Acetone-d_6): δ = 180.81, 180.76, 163.03, 155.20, 152.13, 146.08, 135.19, 134.11, 133.53, 130.04, 129.86, 129.62, 129.48, 127.77, 127.67, 127.24, 126.82, 125.41, 113.79, 102.98, 99.30, 93.16, 91.98, 84.36, 84.30, 82.30, 55.05, 34.61, 30.44, 21.65, 16.75, 13.42, 12.72. ^{19}F NMR (376 MHz, $CDCl_3$): δ = −78.09 (s, 6F, $F_{C–F}$), −145.99 (q, 2F, $F_{B–F}$).

Synthesis of complexes 4 and 6: Compound 2 (30 mg, 0.045 mmol) was dissolved in methanol (20 mL) and $AgCF_3SO_3$ (13 mg, 0.050 mmol) was added to the solution. The reaction mixture was stirred for 1 h at room temperature and filtered to remove AgCl formed. BODIPY (10.7 mg, 0.022 mmol for BDP, 4 and 11.8 mg, 0.023 mmol for BDPCC, 6) was then added to the filtrate and dry nitrogen was bubbled for 10–15 min. The resulting mixture was then stirred for 24 h at room temperature. The solution was reduced to 3 mL and an excess of hexane was slowly layered and kept in refrigerator. The precipitate formed was collected by centrifugation, washed several times with hexane, recrystallized in chloroform and dried in vacuum.

4.2.3. Complex 4

4.2.3.1. Dark pink solid. Yield 21 mg (61%). ESI-MS (CH_3CN): *m/z* = 876.12 $[M - 2CF_3SO_3]^{2+}$. IR (KBr pellets): ν = 2966 (m, C−H); 1608, 1531 (s, C═O, C═C); 1254 (s, CF_3). Anal. calcd for $C_{91}H_{97}O_{12}Ir_2N_4BF_8S_2{\cdot}0.75CHCl_3$: C, 51.50; H, 4.60; N, 2.62. Found: C, 51.55; H, 4.72; N, 2.71. ^{1}H NMR (400 MHz, $CDCl_3$): δ = 8.53 (d, 4H, *J* = 4 Hz, H_α), 7.97 (d, 4H, *J* = 12 Hz, H_a), 7.88 (d, 4H, *J* = 8 Hz, H_b), 7.47 (d, 3H + 4H, *J* = 8 Hz, H_{Ph} + H_c), 7.32 (d, 4H, *J* = 8 Hz, H_β), 7.23 (b, 2H, H_{Ph}), 6.97 (d, 4H, *J* = 12 Hz, H_d), 6.45 (s, 2H, H_e), 3.85 (s, 6H, $OCH_{3,\ AVB}$), 2.47 (s, 6H, $CH_{3,\ BDP}$), 1.59 (s, 30H, cp*), 1.32 (s, 18H, $(CH_3)_{3,\ AVB}$), 1.28 (s, 6H, $CH_{3,\ BDP}$). ^{13}C{^{1}H}-NMR (100 MHz, Acetone-d_6): δ = 178.78, 178.75, 162.62, 154.84, 153.93, 150.09, 144.78, 140.33, 134.97, 129.22, 129.16, 129.01, 127.28, 126.74, 125.14, 122.58, 119.38, 113.48, 92.92, 85.77, 54.61, 34.25, 29.94, 12.21, 11.76, 7.05. ^{19}F NMR (376 MHz, $CDCl_3$): δ = −78.05 (s, 6F, $F_{C–F}$), −145.35 (q, 2F, $F_{B–F}$).

4.2.4. Complex 6

4.2.4.1. Dark pink solid. Yield 27 mg (57%). ESI-MS (CH_3CN): *m/z* = 900.15 $[M - 2CF_3SO_3]^{2+}$. IR (KBr pellets): ν = 2966 (m, C−H); 2202 (m, C≡C); 1605, 1518 (s, C═O, C═C); 1258 (s, CF_3). Anal. calcd for $C_{95}H_{97}O_{12}Ir_2N_4BF_8S_2{\cdot}CHCl_3$: C, 52.00; H, 4.45; N, 2.53. Found: C, 51.95; H, 4.52; N, 2.56. ^{1}H NMR (400 MHz, $CDCl_3$): δ = 8.46 (d, 4H, *J* = 8 Hz, H_α), 7.96 (d, 4H, *J* = 8 Hz, H_a), 7.87 (d, 4H, *J* = 8 Hz, H_b), 7.48 (m, 11H, H_{Ph} + H_c + H_β), 7.21 (m, 2H, H_{Ph}), 6.97 (d, 4H, *J* = 8 Hz, H_d), 6.42 (s, 2H, H_e), 3.86 (s, 6H, $OCH_{3,\ AVB}$), 2.61 (s, 6H, $CH_{3,\ BDP}$), 1.61 (s, 30H, cp*), 1.44 (s, 6H, $CH_{3,\ BDP}$), 1.33 (s, 18H, $(CH_3)_{3,\ AVB}$). ^{13}C{^{1}H}-NMR (100 MHz, Acetone-d_6): δ = 179.14, 179.10, 163.11, 155.36, 150.61, 150.57, 135.37, 129.64, 129.47, 127.87, 127.67, 127.23, 127.19, 125.59, 125.31, 113.96, 93.39, 86.20, 55.08, 34.67, 30.42, 12.75, 12.72, 7.61. ^{19}F NMR (376 MHz, $CDCl_3$): δ = −78.08 (s, 6F, $F_{C–F}$), −145.94 (q, 2F, $F_{B–F}$).

4.3. Biological experiments

4.3.1. MTT assay

Mouse embryo fibroblast cell line (NIH 3T3) and cancer cells (MCF-7, HeLa, A549) were purchased from American Type Culture Collection (Rockville, MD) and National Centre for Cell Sciences, India respectively. They were cultured according to the supplier's recommendations. To study the cytotoxicity of the synthesized complexes, after 80% confluence, cells were trypsinized with 0.1% trypsin-EDTA and harvested by centrifugation at 500 x g. Serial dilutions of cells were made from 1×10^6 to 1×10^3 cells per ml. The cells were seeded in triplicate in a 96 well plate. The suspended cells were treated with 1, 3, 5, 7, 10 μM of complexes 5 and 6 for 24 h duration. Since ***doxorubicin*** was known as potential anticancer drug, the fibroblast and tumor cells were treated with ***doxorubicin, in the same concentration range*** (1 μM–10 μM) were considered as control. The cell viability was determined by measuring the ability of cells to transform MTT to a purple colored formazan dye. The absorbance of samples at 570 nm was measured using a UV–Visible spectrophotometer. Percentage of viable cells was calculated by using the formula given below.

$$\textbf{Percentage of cell viability} = \frac{\textbf{OD}_{570}\ \textbf{Sample}}{\textbf{OD}_{570}\ \textbf{Control s}} \times \textbf{100}$$

where the OD_{570} (sample) corresponds to absorbance obtained from the wells treated with complexes and OD_{570} (control) represents the absorbance from the wells in which no complex was added.

4.3.2. UV–Visible spectroscopy

UV–Visible absorption spectra were recorded using ABI Lambda Spectrophotometer (Waltham, MA, USA) at 25 °C. All the experiments were carried out in polystyrene cuvettes to minimize binding of complexes to the surface of the cuvettes. 5.0 μM of complexes 5 and 6 was prepared in DMSO and 5.0 μM of CT-DNA in 100 mM Tris buffer (pH 7.0). Each complex was added to 1 ml Milli Q water taken in 1 cm path length cuvette and absorption spectra were recorded in the range of 300 nm to 400 nm after the subsequent additions of 5 μl CT-DNA. All the solutions were freshly prepared before starting the experiment and titration was carried out until saturation of absorbance.

4.3.3. Fluorescence spectroscopic titrations

Fluorescence emission spectra were measured at 25 °C using a Hitachi F4500 spectrofluorimeter (Maryland, USA) using a 1 cm path length quartz cuvette. Quartz cuvettes was thoroughly washed with distilled water and dilute nitric acid (~0.1 N) to minimize non-specific binding of the molecules to the surface of the cuvette. Throughout the fluorescence experiment, the concentration of the complexes was kept constant (10 μM) and titrated with increasing concentrations of CT-DNA (multiples of 0.005 μM). Fluorescence spectra were recorded after

each addition of CT-DNA to the fluorescent cuvette. After each experiment, the quartz cuvettes was thoroughly washed with distilled water and dilute nitric acid (~0.1 N) to remove traces of molecules binding to the walls of quartz cuvette. Complexes 5 and 6 were excited at 440 nm, and emission spectra for each titration were recorded sin the wavelength range from starting from 550 nm to 615 nm. Each spectrum was recorded three times and the average of three scans was taken.

4.3.4. Circular dichroism (CD) spectroscopy

Circular dichroism experiments were performed using a JASCO 815 CD Spectro polarimeter (Jasco, Tokyo, Japan). The solution of CT-DNA was prepared in 100 mM Tri buffer. To 10 μM of CT-DNA, 10 and 20 μM of complexes 5 and 6 were added. The CD spectra were recorded from 230 nm to 330 nm in 1 mm path length cuvette. The spectra were averaged over 3 scans, which were recorded at 100 nm/min with a response time of 1 s and a band width of 1 nm.

4.3.5. Cell cycle analysis by flow cytometry

In cancer cells, the cell cycle is often deregulated and undergo unscheduled cell divisions. Therefore, inhibition of cell cycle provides an opportunity to identify a suitable molecule to treat proliferative diseases like cancer. For cell cycle assay, complexes 5 and 6 was chosen as it was earlier shown that these complexes are cytotoxic (with the MTT assay). This assay was performed to assess the effect of complexes 5 and 6 on different stages of the cell cycle. Flow cytometry experiments were carried out by following the protocol reported earlier [9k]. As complexes 5 and 6 were showing maximum cytotoxic effect on MCF-7 cells, they were incubated with 1.0 μM and 5.0 μM concentrations of 5 and 6 for 48 h. Untreated MCF-7 cells were used as control. Untreated and treated cells were harvested, washed with phosphate buffered saline (PBS), fixed in ice-cold 70% alcohol and stained with propidium iodide (PI) (Sigma Aldrich). The cell cycle assay was performed using Becton Dickinson FACSCaliber flow cytometer.

4.3.6. Apoptosis assay

1×10^6 MCF-7 cells were treated with 1.0 μM and 5.0 μM of complexes 5 and 6 for 24 h and subsequently washed with 2× binding buffer and resuspended in 100 μl binding buffer and Annexin-V-FITC from Abcam (1.0 μg). The cells were then incubated at room temperature for 10 min, followed by the addition of 400.0 μl of binding buffer containing 1.0 μl of propidium iodide (PI) (Sigma Aldrich). Stained cells were analyzed using a FACSCalibur flow cytometer from B.D Biosciences. Annexin-V-FITC and PI labeled cells were excited using a 488 nm solid-state laser, and fluorescence emission intensity of FITC and PI were captured using 530/30 and 585/42 band-pass filters, respectively.

4.3.7. Immunofluorescence/confocal microscopic studies

10,000 MCF-7 cells were seeded on 18-mm cover slips and incubated for 24 h. After incubation, cells were treated with complexes 5 and 6, at 1.0 μM and 5.0 μM concentration for 48 h. Hoechst 33258 (Sigma Aldrich) was added to the cells at a concentration of 0.5 mg/ml and incubated for 30 min at 37 °C. Later, HeLa cells were rinsed with PBS. Cells from each cover slip were captured from randomly selected fields under a confocal microscope (Leica TCS SP5, Heidelberg, Germany) to qualitatively determine the proportion of viable and apoptotic cells based on their relative fluorescence, cell morphology and nuclear fragmentation.

4.3.8. Mitochondria outer membrane permeability assay

MCF-7 cells were treated with complexes 5 and 6 (5 μM each) and incubated with Mitotracker Red (50 nM) for 30 min at culture conditions recommended by the supplier. Cells devoid of any treatment were considered as control. Cells were washed and fixed with 4% paraformaldehyde for 15 min, and permeabilized with Triton X-100 (0.1%) for each 10 min. The cover glasses after PBS wash were mounted on to the glass slides and observed using laser scanning confocal microscopy (Leica TCS SP5, Heidelberg, Germany). The Mitotracker Red was excited using 543 nm laser source and the fluorescence emission signals were collected at 570 nm to 635 nm.

Abbreviations

AVBH	(1-(4-*tert*-butylphenyl)-3-(4-methoxyphenyl)propane-1,3-dione
BDP	4-dipyridine boron dipyrromethene
BDPCC	4-ethynylpyridine boron dipyrromethene
p-cym	para-cymene
DFT	Density Functional Theory
MLCT	Metal-to-Ligand Charge-Transfer
PCM	Polarizable Continuum Model
IEFPCM	Integral Equation Formalism Polarizable Continuum Model
CT-DNA	Calf-Thymus Deoxyribonucleic Acid

Acknowledgements

This research was supported by a Post-Doctoral Research Program (2018) for GG through Incheon National University, Incheon, Republic of Korea. This research was also supported by mid-career researcher programs of the National Research Foundation of Korea funded by the Ministry of Science, ICT & Future Planning (NRF-2016R1A2B4010376).

Appendix A. Supplementary data

Supplementary data to this article can be found online at https://doi.org/10.1016/j.jinorgbio.2018.08.009.

References

[1] B. Demoro, R.F.M. de Almeida, F. Marques, C.P. Matos, L. Otero, J.C. Pessoa, I. Santos, A. Rodríguez, V. Moreno, J. Lorenzo, D. Gambino, A.I. Tomaz, Dalton Trans. 42 (2013) 7131–7146.
[2] (a) L. Kelland, Nat. Rev. Cancer 7 (2007) 573–584;
(b) B. Rosenberg, L.V. Camp, T. Krigas, Nature 205 (1965) 698–699;
(c) Y. Jung, S.J. Lippard, Chem. Rev. 107 (2007) 1387–1407;
(d) J. Reedijk, Eur. J. Inorg. Chem. (2009) 1303–1312.
[3] P.C.A. Bruijnincx, P.J. Sadler, Curr. Opin. Chem. Biol. 12 (2008) 197–206.
[4] (a) L. Ronconi, P.J. Sadler, Coord. Chem. Rev. 251 (2007) 1633–1648;
(b) S.H. van Rijt, P.J. Sadler, Drug Discov. Today 14 (2009) 1089–1097;
(c) K.J. Kilpin, S. Crot, T. Riedel, J.A. Kitchen, P.J. Dyson, Dalton Trans. 43 (2014) 1443–1448.
[5] (a) K.J. Kilpin, P.J. Dyson, Chem. Sci. 4 (2013) 1410–1419;
(b) E. Meggers, Chem. Commun. (2009) 1001–1010;
(c) M. Patra, G. Gasser, ChemBioChem 13 (2012) 1232–1252;
(d) V. Brabec, O. Nováková, Update 9 (2006) 111–122;
(e) C. Mari, V. Pierroz, S. Ferrari, G. Gasser, Chem. Sci. 6 (2015) 2660–2686.
[6] (a) G. Süss-Fink, Dalton Trans. 39 (2010) 1673–1688;
(b) G.S. Smith, B. Therrien, Dalton Trans. 40 (2011) 10793–10800;
(c) G. Süss-Fink, J. Organomet. Chem. 751 (2014) 2–19;
(d) A.K. Singh, D.S. Pandey, Q. Xu, P. Braunstein, Coord. Chem. Rev. 270-271 (2014) 31–56;
(e) P.J. Dyson, G. Sava, Dalton Trans. (2006) 1929–1933;
(f) R. Chakrabarty, P.S. Mukherjee, P.J. Stang, Chem. Rev. 111 (2011) 6810–6918;
(g) S.K. Singh, D.S. Pandey, RSC Adv. 4 (2014) 1819–1840;
(h) L. Ronconi, P.J. Sadler, Coord. Chem. Rev. 251 (2007) 1633–1648.
[7] (a) G. Mestroni, E. Alessio, M. Calligaris, W.M. Attia, F. Quadrifoglia, S. Cauci, G. Sava, S. Zorzet, S. Pacor, C. Monti-Bragadin, M. Tamaro, L. Dolzani, Chemical, Biological and Antitumor Properties of Ruthenium(II) Complexes With Dimethylsulfoxide. Progress in Clinical Biochemistry and Medicine, Vol. 10 Springer-Verlag, Berlin, Hiedelberg, 1989, p. 71;
(b) C.G. Hartinger, S. Zorbas-Seifried, M.A. Jakupec, B. Kynast, H. Zorbas, B.K. Keppler, J. Inorg. Biochem. 100 (2006) 891–904;
(c) R. Trondl, P. Heffeter, C.R. Kowol, M.A. Jakupec, W. Berger, B.K. Keppler, Chem. Sci. 5 (2014) 2925–2932.
[8] (a) C. Santini, M. Pellei, V. Gandin, M. Porchia, F. Tisato, C. Marzano, Chem. Rev. 14 (2014) 815–862;
(b) N. Farrell, Metal Complexes as Drugs and Chemotherapeutic Agents. Comprehensive Coordination Chemistry II, Vol. 9, pp. 809–840;
(c) D.M. Koegan, D.M. Griffith, Molecules 19 (2014) 15258–15297;
(d) S. Spreckelmeyer, C. Orvig, A. Casini, Molecules 19 (2014) 15584–15610;
(e) I. Ott, Coord. Chem. Rev. 253 (2009) 1670–1681;
(f) C.R. Munteanu, K. Suntharalingam, Dalton Trans. 44 (2015) 13796–13808;
(g) W.A. Wani, U. Baig, S. Shreaz, R.A. Shiekh, P.R. Iqbal, E. Jameel, A. Ahmad, S.

H. Mohd-Setapar, M. Mushtaque, L.T. Hun, New J. Chem. 40 (2016) 1063–1090
[9] (a) Z. Liu, I. Romero-Canelón, B. Qamar, J.M. Hearn, A. Habtemariam, N.P.E. Barry, A.M. Pizarro, G.J. Clarkson, P.J. Sadler, Angew. Chem. Int. Ed. 53 (2014) 3941–3946;
(b) Z. Liu, A. Habtemariam, A.M. Pizarro, G.L. Clarkson, P.J. Sadler, Organometallics 30 (2011) 4702–4710;
(c) J.M. Hearn, I. Romero-Canelón, B. Qamar, Z. Liu, I. Hands-Portman, P.J. Sadler, ACS Chem. Biol. 8 (2013) 1335–1343;
(d) Z. Liu, A. Habtemariam, A.M. Pizarro, S.A. Fletcher, A. Kisova, O. Vrana, L. Salassa, P.C.A. Bruijnincx, G.J. Clarkson, V. Brabec, P.J. Sadler, J. Med. Chem. 54 (2011) 3011–3026;
(e) G. Gupta, J.M. Kumar, A. Garci, N. Nagesh, B. Therrien, Molecules 19 (2014) 6031–6046;
(f) G. Gupta, A. Das, N.K. Ghate, T. Kim, J.Y. Ryu, J. Lee, N. Mandal, C.Y. Lee, Chem. Commun. 52 (2016) 4274–4277;
(g) G. Gupta, G.S. Oggu, N. Nagesh, K.K. Bokara, Therrien, CrystEngComm 18 (2016) 4952–4957;
(h) G. Gupta, E. Denoyelle-Di-Muro, J.-P. Mbakidi, S. Leroy-Lhez, V. Sol, B. Therrien, J. Organomet. Chem. 787 (2015) 44–50;
(i) P. Zhang, P.J. Sadler, J. Organomet. Chem. 839 (2017) 5–14;
(j) G. Gupta, J.M. Kumar, A. Garci, N. Rangaraj, N. Nagesh, B. Therrien, ChemPlusChem 79 (2014) 610–618;
(k) J.P. Johnpeter, G. Gupta, J.M. Kumar, G. Srinivas, N. Nagesh, B. Therrien, Inorg. Chem. 52 (2013) 13663–13673;
(l) G. Gupta, A. Garci, B.S. Murray, P.J. Dyson, G. Fabre, P. Trouillas, F. Giannini, J. Furrer, G. Süss-Fink, B. Therrien, Dalton Trans. 42 (2013) 15457–15463.
[10] (a) W. Kandioller, E. Balsano, S.M. Meier, U. Jungwirth, S. Göschl, A. Roller, M.A. Jakupec, W. Berger, B.K. Keppler, C.G. Hartinger, Chem. Commun. 49 (2013) 3348–3350;
(b) G. Agonigi, T. Riedel, S. Zacchini, E. Păunescu, G. Pampaloni, N. Bartalucci, P.J. Dyson, F. Marchetti, Inorg. Chem. 54 (2015) 6504–6512;
(c) A. Kurzwernhart, W. Kandioller, C. Bartel, S. Bächler, R. Trondl, G. Mühlgassner, M.A. Jakupec, V.B. Arion, D. Marko, B.K. Keppler, C.G. Hartinger, Chem. Commun. 48 (2012) 4839–4841;
(d) A. Kurzwernhart, W. Kandioller, S. Bächler, C. Bartel, S. Martic, M. Buczkowska, G. Mühlgassner, M.A. Jakupec, H.B. Kraatz, P.J. Bednarski, V.B. Arion, D. Marko, B.J. Keppler, J. Med. Chem. 55 (2012) 10512–10522;
(e) J. Du, Y. Kang, Y. Zhao, W. Zheng, Y. Zhang, Y. Lin, Z. Wang, Y. Wang, Q. Luo, K. Wu, F. Wang, Inorg. Chem. 55 (2016) 4595–4605.
[11] (a) R. Pettinari, F. Marchetti, A. Petrini, C. Pettinari, G. Lupidi, P. Smoleński, R. Scopelliti, T. Riedel, P.J. Dyson, Organometallics 35 (2016) 3734–3742;
(b) P.A.D.S. Abranches, E.D. da Silva, E.V.V. Varejão, C.V.B. Martins, A.L.T.G. Ruiz, M.A. de Resende-Stoianoff, J.E. de Carvalho, Â. de Fátima, S.A. Fernandes, Lett. Drug Des. Discovery 10 (2013) 661–665.
[12] (a) G. Gupta, A. Das, K.C. Park, A. Tron, H. Kim, J. Mun, N. Mandal, K.-W. Chi, C.Y. Lee, Inorg. Chem. 56 (2017) 4615–4621;
(b) G. Gupta, A. Das, S. Panja, J.Y. Ryu, J. Lee, N. Mandal, C.Y. Lee, Chem. Eur. J. 23 (2017) 17199–17203;
(c) N. Boens, V. Leen, W. Dehaen, Chem. Soc. Rev. 41 (2012) 1130–1172;
(d) M.S.T. Goncalves, Chem. Rev. 109 (2009) 190–212;
(e) E.R. Thapaliya, Y. Zhang, P. Dhakal, A.S. Brown, J.N. Wilson, K.M. Collins, F.M. Raymo, Bioconjug. Chem. 28 (2017) 1519–1528;
(f) L. Yuan, W. Lin, K. Zheng, L. He, W. Huang, Chem. Soc. Rev. 42 (2013) 622–666;
(g) G. Gupta, A. Das, J. Lee, N. Mandal, C.Y. Lee, ChemPlusChem 83 (2018) 339–347.
[13] (a) J.D. Chai, M. Head-Gordon, Phys. Chem. Chem. Phys. 10 (2008) 6615–6620;
(b) M.J. Frisch, G.W. Trucks, H.B. Schlegel, G.E. Scuseria, M.A. Robb, J.R. Cheeseman, G. Scalmani, V. Barone, B. Mennucci, G.A. Petersson, H. Nakatsuji, M. Caricato, X. Li, H.P. Hratchian, A.F. Izmaylov, J. Bloino, G. Zheng, J.L. Sonnenberg, M. Hada, M. Ehara, K. Toyota, R. Fukuda, J. Hasegawa, M. Ishida, T. Nakajima, Y. Honda, O. Kitao, H. Nakai, T. Vreven, J.A. Montgomery Jr., J.E. Peralta, F. Ogliaro, M. Bearpark, J.J. Heyd, E. Brothers, K.N. Kudin, V.N. Staroverov, R. Kobayashi, J. Normand, K. Raghavachari, A. Rendell, J.C. Burant, S.S. Iyengar, J. Tomasi, M. Cossi, N. Rega, J.M. Millam, M. Klene, J.E. Knox, J.B. Cross, V. Bakken, C. Adamo, J. Jaramillo, R. Gomperts, R.E. Stratmann, O. Yazyev, A.J. Austin, R. Cammi, C. Pomelli, J.W. Ochterski, R.L. Martin, K. Morokuma, V.G. Zakrzewski, G.A. Voth, P. Salvador, J.J. Dannenberg, S. Dapprich, A.D. Daniels, Ö. Farkas, J.B. Foresman, J.V. Ortiz, J. Cioslowski, D.J. Fox, Gaussian 09, Revision E.01, Gaussian, Inc., Wallingford CT, 2009;
(c) T. Kim, N. Singh, J. Oh, E.-H. Kim, J. Jung, H. Kim, K.-W. Chi, J. Am. Chem. Soc. 138 (2016) 8368–8371;
(d) Y.H. Song, N. Singh, J. Jung, H. Kim, E.-H. Kim, H.-K. Cheong, Y. Kim, K.-W. Chi, Angew. Chem. Int. Ed. 55 (2016) 2007–2011;
(e) P.J. Hay, W.R. Wadt, J. Chem. Phys. 82 (1985) 299;
(f) C. Adamo, V. Barone, J. Chem. Phys. 110 (1999) 6158.
[14] Z.-Q. Liu, Y.-T. Li, Z.-Y. Wu, S.-F. Zhang, Inorg. Chim. Acta 362 (2009) 71–77.
[15] L. Wang, Y. Wen, J. Liu, J. Zhou, C. Li, C. Wei, Org. Biomol. Chem. 9 (2011) 2648–2653.
[16] H. Fukuda, M. Katahira, N. Tsuchiya, Y. Enokizono, T. Sugimura, M. Nagao, H. Nakagama, Proc. Natl. Acad. Sci. U. S. A. 99 (2002) 12685–12690.
[17] M. Kajstura, H.D. Halicka, J. Pryjma, Z. Darzynkiewicz, Cytometry A 71 (2007) 125–131.
[18] A.H. Wyllie, Nature 284 (1980) 555–556.
[19] R.W. Larsen, R. Jasuja, R.K. Hetzler, P.T. Muraoka, V.G. Andrada, D.M. Lameson, Biophys. J. 70 (1996) 443–452.
[20] J. Piosik, M. Zdunek, J. Kapuscinski, Biochem. Pharmacol. 63 (2002) 635–646.
[21] M.B. Lyles, I.L. Cameron, Biophys. Chem. 96 (2002) 53–76.
[22] F. Traganos, J. Kapuscinski, Z. Darzynkiewicz, Cancer Res. 51 (1991) 3682–3689.
[23] N. Haga, N. Fujita, T. Tsuruo, Oncogene 22 (2003) 5579–5585.